Wind and Structures, Vol. 15, No. 1 (2012) 43-64
DOI: http://dx.doi.org/10.12989/was.2012.15.1.043

A neural network shelter model for small wind turbine siting near single obstacles

Andrew William Brunskill and William David Lubitz*

University of Guelph, School of Engineering. 50 Stone Road East, Guelph, Ontario, Canada. N1G 2W1
(Received July 20, 2010, Revised January 27, 2011, Accepted May 25, 2011)

Abstract. Many potential small wind turbine locations are near obstacles such as buildings and shelterbelts, which can have a significant, detrimental effect on the local wind climate. A neural network-based model has been developed which predicts mean wind speed and turbulence intensity at points in an obstacle's region of influence, relative to unsheltered conditions. The neural network was trained using measurements collected in the wakes of 18 scale building models exposed to a simulated rural atmospheric boundary layer in a wind tunnel. The model obstacles covered a range of heights, widths, depths, and roof pitches typical of rural buildings. A field experiment was conducted using three unique full scale obstacles to validate model predictions and wind tunnel measurements. The accuracy of the neural network model varies with the quantity predicted and position in the obstacle wake. In general, predictions of mean velocity deficit in the far wake region are most accurate. The overall estimated mean uncertainties associated with model predictions of normalized mean wind speed and turbulence intensity are 4.9% and 12.8%, respectively.

Keywords: wind tunnel; small wind turbine; wind energy; micrositing; wake prediction; anemometer; sheltering; neural network.

1. Introduction

Knowledge of the flow around bluff bodies in the atmospheric boundary layer (ABL) is relevant to a wide range of fields including structural engineering, airborne contaminant dispersion, and the development and implementation of wind turbines. Accurate prediction of the wind field in the regions near buildings and other obstacles is particularly important when micrositing (determining the optimum turbine location within a small area) a small wind turbine (SWT). The power production of a SWT is proportional to the cube of the wind speed over much of its operating range. In practice, SWTs are often sited close to buildings or other obstacles, potentially resulting in significant performance degradation due to reduced mean wind speeds and increased turbulence at the SWT location.

The most common method of micrositing a small turbine is to use one of several general guidelines that prescribe a region near obstacles where a SWT should not be located. One of the most common of these guidelines is that a small turbine should be at least 20 obstacle heights downwind, and at a height greater than twice that of the obstacle (U.S. Department of Energy

* Corresponding author, Assistant professor, Email: wlubitz@uoguelph.ca

2005). Several similar guidelines specifying a range of avoidance regions are described in Brunskill (2010). Although useful, general guidelines are oversimplified, and often inadequate. Obstacle geometry is specified only in terms of height, omitting other important characteristics such as obstacle width, which has been shown to have a major effect on the size and extents of the obstacle wake region (Peterka 1985). Guidelines are generally based on experience, but since each site is unique, what is suitable at one site may not be at another site. Potentially, the use of guidelines may result in the exclusion of many sites which are well suited for a SWT, or the inclusion of sites where the turbine would still experience significant detrimental wake effects. For example, experimental evidence from a wind tunnel study by Lemberg (1973) indicates that the turbulence intensity excess in the wake of a cube decays slowly, and can be seen at downwind distances as great as 50 cube heights. If a small turbine were to be placed 25 heights downwind of a cubic building, which is acceptable according to the "20 heights downwind, 2 heights high" rule cited above, it may still experience turbulence levels higher than ambient, which could be detrimental to the turbine's power output and lifespan. Simple guidelines that prescribe a specific region to avoid placing a wind turbine give no guidance on the effects of incrementally changing the SWT location, since no attempt is made to predict the flow field.

A series of models that predict the flow field near an obstacle have been developed over the past several decades. As reported by Lemberg (1973), Hunt and Smith developed a momentum-wake theory to provide quantitative predictions of the velocity deficit in the wake of a three-dimensional obstacle. To simplify the governing flow equations, they assumed that the velocity deficit was small, which means that their theory is only valid for the far wake region. Two constant eddy viscosities were used, for the lateral and vertical directions. These were expressed as a fraction of the eddy viscosity of the incoming flow; thus, eddy viscosities were calculated from properties of the incident boundary layer. Predictions made by the model developed using this theory agreed reasonably well with Counihan's data (Lemberg 1973) for the wake behind a cube. However, it was necessary to specify values of two parameters in order to obtain the best fit of predictions to measured data.

Counihan *et al*. (1974) state that the wake strength can be described by the downwind component of the moment of momentum deficit, which is constant throughout the far wake. Hunt and Smith (as reported by Lemberg 1973) incorporated this "wake moment" into their model, which is related to the overturning moment on the obstacle from the wind. The wake moment is a measure of the pressure forces acting on the obstacle and the surface near the obstacle, and relates wake flow in the far field to the pressure field close to the obstacle. Although wake moment is not equal to overturning moment, Lemberg states that they will be similar for three dimensional obstacles (Lemberg 1973).

Based on the theories of Hunt and Smith, Lemberg (1973) created a more general model incorporating an expression for eddy viscosity as a power law function of height above the ground, and setting eddy viscosity proportional to the height and frontal width of the obstacle. Experimentally determined power law constants were used to predict how eddy viscosity varies throughout the flow; however, in practice, values of these coefficients are difficult to determine (Musselman 1996). As in the theory of Hunt and Smith, the forms of the velocity profiles in the vertical and lateral directions must be assumed.

Perera (1981) developed a set of empirical correlations which estimate the velocity deficit and Reynolds stresses at any point downstream of a two-dimensional porous fence. These correlations are based on measurements made during wind tunnel tests, similar to those carried out by Counihan *et al*. (1974). Perera's (1981) correlations are expressed in terms of self-preserving, non-

dimensionalized variables. A version of Perera's model adapted to predict the wakes of three-dimensional obstacles forms the basis of the WAsP sheltering model (Troen and Petersen 1989).

Based largely on the work of Lemberg (1973), Counihan *et al*. (1974), and Perera (1981),Taylor and Salmon (1993) developed a model to correct anemometer measurements for sheltering by upwind obstacles. Their model can be used to estimate the velocity deficit that would be observed by an anemometer at a specified location in an obstacle wake. Model inputs are the length, width, and height of the obstacle, the wake moment coefficient $\tilde{C}_h$ (which is assumed to be roughly equal to the overturning moment on the obstacle), its position upstream of an anemometer site, and the local surface roughness. Since the velocity deficit is assumed to be small, the model predictions are limited to the far wake region, described by Lemberg (1973) as starting approximately $5\,h$ downwind of the obstacle, where h is the height of the obstacle. (Other authors use different definitions for the start of the far wake. For example, Perera (1981) assumes the far wake begins roughly $7.5\,h$ downwind of a wall. In fact, the start of the far wake will be dependent on the characteristics of the obstacle.) Taylor and Salmon (1993) also assumed functional forms of the velocity deficit in the vertical and lateral directions. The vertical self-similar profile is based on the work of Perera (1981), while the lateral velocity deficit is assumed to be symmetrical with a Gaussian form. This may be a reasonable approximation for flow fields around simple geometries, such as the flow around a cube oriented normal to the wind. For more complicated flows, such as around a block with an azimuth of 47^{o} to the wind direction, the velocity deficit distribution is neither Gaussian nor symmetric (Hansen 1975, Peterka 1985). Taylor and Salmon (1993) caution that they did not consider the 'vortex wake', and state that when present, standing vortices could lead to velocity deficits significantly different than those predicted by their model. As discussed by Hansen *et al*. (1975), standing vortices are formed in the wake when the obstacle is presenting prominent edges to the wind direction. This implies that although Taylor and Salmon's (1993) model is suitable for simple cases, such as a cubic obstacle with its front face normal to the flow, predictions may be poor when standing vortices are present, as occurs when the obstacle's front face is not normal to the flow. Another important issue for wind turbine micrositing is that Taylor and Salmon's (1993) model predicts only mean wind speeds, and does not provide guidance regarding turbulence levels in obstacle wakes.

Recall that the purpose of the new model developed in this study is to provide guidance regarding small wind turbine micrositing near obstacles. A simple way of predicting velocity deficit and turbulence intensity excess in an obstacle's region of influence is needed. In later sections, it is shown that existing theoretically-derived models are of poor accuracy for many common flows. It was felt that an empirical approach was more promising for a practical application such as small wind turbine micrositing. A neural network (NN)-based wind model is empirical because it is based entirely on experimental velocity measurements. Creating a model based on a relationship learned using NNs is a form of non-linear regression. The NN approach was chosen over other non-linear regression methods mainly because a NN has the ability to adapt when presented with new information. In this way, a NN model has the potential to continually become better at solving a problem over time.

Neural networks have been used extensively to empirically model complex relationships between two or more variables, including for wind engineering problems. Bitsuamlak *et al*. (2006, 2007) used a NN approach to predict wind speed-up over single and multiple hills. Five model inputs were used: (i) the windward slope of the hill, (ii) the roughness length of the ground, (iii) the hill type (single or multiple), (iv) the distance between the hills (when multiple hills are present), and

(v) the height of interest above the hill. Training data was generated using CFD simulations of flow over hills with k-ε turbulence closure. The use of NNs allowed the possibility of making the model available to end users, who would be able to predict speed-up just by entering appropriate input values. Bitsuamlak *et al*.'s (2006) NN speed up predictions compared well with an independent set of experimental data, including predictions made for cases not in the training data. They concluded that for the end user the NN approach is less expensive than CFD simulations alone while producing results of comparable accuracy.

Zhang *et al*. (2004) developed a NN-based model that predicts how the wind loads on a building are influenced by the presence of a second nearby building with identical footprint. The model had four inputs (two defining the space between the two buildings, the ratio of building heights, and the local surface roughness) and output the interference factor, defined as the ratio of the load on the first building when the second building is present to the load when no other buildings are present. A total of 106 data points were available, taken from a variety of experimental sources. 80% of the data was used as training data, while the remaining 20% was used for validation. The NN was able to predict the interference factor with good accuracy. Similarly, Khanduri *et al*. (1997) proposed the use of backpropogation neural networks to estimate the wind load on a building while accounting for the interference effects caused by adjacent buildings.

Chen *et al*. (2003) describe a NN approach to the prediction of pressure coefficients on the roofs of low buildings. Two backpropogation NNs were trained using wind tunnel data and the Levenberg-Marquardt training algorithm (also used here, as discussed in Section 2.1). Each NN had four inputs and a single output. This arrangement is similar to the NN trained in the current paper. Chen *et al*. found that the mean square errors of all pressure taps in the corner of the building were 12% and 9% for the mean and root-mean-square coefficients, respectively.

2. Methodology

2.1 Neural network

Neural networks were identified as a promising method for developing a new model to predict mean velocity deficit and turbulence intensity at specific locations near obstacles. The new model developed here is referred to as Wakenet. There are two types of model inputs: those describing obstacle geometry, and those defining the point at which wind speed and turbulence intensity are to be predicted by the model. The three inputs defining the point of interest in the wake are the downwind position x, lateral position z, and height above ground y. Note that x, y and z are non-dimensional distances that have been normalized by the obstacle height h. The coordinate system origin is at the center of the obstacle model. Model inputs are illustrated in (Fig. 1) .

An obstacle's size is described by its width w, depth d, and height h. w and d are constant for each obstacle, and independent of model orientation, since they are defined for the case where wind is normal to the front face of the obstacle. The four model inputs describing the obstacle are its aspect ratio $AR = w/h$, plan ratio $PR = d/h$, orientation relative to the wind a, and roof pitch RA. The AR of the obstacle has a major influence on its wake (Hansen *et al*. 1975, Martinuzzi and Tropea 1993, Musselman 1996). The effect of PR on the wake region is much less studied. Compared to AR, it is appears that PR has a smaller but still significant effect on the wake of an obstacle in the ABL. For example, it is known that PR is a factor in whether the flow reattaches to

the top of the obstacle, or to the ground further downwind (Peterka 1985). Note that these definitions apply to prismatic obstacles, which are the main interest in this study.

The orientation angle of the model with respect to wind direction a has a dramatic effect on the wake (Hansen 1975). In a way, each unique a value represents a new obstacle; for each orientation angle, the position and orientation of obstacle edges and faces are different relative to the wind. As previously noted, the way in which this differing geometry interacts with the wind results in different wake structures as a changes.

One way in which Hunt and Smith (Lemberg 1973) were able to improve upon previous models was by taking into consideration the wake moment coefficient. Taylor and Salmon (1993) also used wake moment coefficient $\tilde{C}_h$ as an input for their model as it is a better measure of wake strength than drag coefficient. As noted by Taylor and Salmon (1993), the value of $\tilde{C}_h$ will be affected by the shape of the obstacle. $\tilde{C}_h$ was considered as a potential Wakenet input. However, it would be very difficult for the average wind turbine owner to accurately measure or estimate the wake moment of nearby obstacles, meaning that the inclusion of $\tilde{C}_h$ as a model input would not satisfy the criterion that the model be simple to use. Instead of $\tilde{C}_h$ the roof angle (or pitch) RA was selected as a model input to represent the shape of the obstacle. $\tilde{C}_h$ for buildings with simple geometry. RA is defined as the angle of roof surface above horizontal (a peaked or gable roof geometry is assumed with the roof ridgeline parallel to the obstacle front face, so that the length of the roof ridgeline from one end of the obstacle to the other is w). RA can be thought of as an easier-to-determine proxy for $\tilde{C}_h$ for buildings with simple geometry.

The Wakenet model was trained and evaluated using the MATLAB Neural Network Toolbox. Wind tunnel measurements of flow around obstacles were used as training data. The database of wind tunnel data was greatly expanded from the 4473 points that were directly measured by making assumptions regarding the values of R_V and R_I at certain points in the wake. Three methods were used to make these assumptions. The first was to define boundary conditions for extreme positions in the wake. For example, in the wake of a block with $AR = 4$, $PR = 1$, $RA = 0$, oriented at an angle of 23°, R_V was measured to be 0.98 and 0.99 at (x, y, z) = (10, 2.9, −1.6) and (10, 3.4, −1.6), respectively. From these values it was assumed that R_V had a value of 1.00 at 10, 4, -1.6). The database was also expanded utilizing symmetry. Although the wake of an obstacle is not symmetrical for most obstacle orientations, symmetry can still be applied by changing the sign of the model orientation a and the lateral position z of the point of interest, creating a mirrored set of data. The third way in which training points were generated comes from the understanding that a block with an AR of 1 and a PR of 4 is the same as a block with an AR of 4 and a PR of 1, when the former is rotated 90°. (This is only true when $RA = 0°$.) Any point in the wake of a flat block can be used to generate a duplicate point by swapping AR and PR, adding 90° to a, and using the same output values for R_V and R_I. These three techniques were used to expand the wind tunnel wake effects database from 4473 to 42166 points. Applying the assumed values during post-processing, which would reduce NN training time, was considered but it was found that the additional training data made available by making these assumptions improved the accuracy and generality of the network's predictions.

There are two main categories of measurements in the wake effects database. 'Training pool' measurements were collected using 'training' obstacles, as described in . This training pool was randomly divided into actual training data (random 90%, 37504 points) and validation data (remaining 10%, 4168 points). The second main category of points, the 'pure' validation data, consisted of measurements which were collected using 'validation' obstacles (494 points in total).

These measurements were not used as training data. A subset of the pure validation set contains points where $x > 5$, $y > 1$. This subset is referred to as far wake pure validation data (279 points).

During model development, it was found that recasting some inputs into other forms resulted in more accurate NN models. For the final version of Wakenet, thirteen NN inputs were calculated using the seven original model inputs (*AR, PR, RA, a, x, y, z*). Model orientation angle *a* was replaced as an input with two new inputs; (i) the sine and ii) the cosine of *a*. *RA* was similarly replaced by the sine and cosine of *RA*. Four new inputs were added; (i) lateral distance between the transverse position, *z*, and the close lateral edge of the obstacle, (ii) the lateral distance between the transverse position, *z*, and the far lateral edge of the obstacle, (iii) the longitudinal distance between the downwind position, *x*, and the most upwind edge of the obstacle, and (iv) the longitudinal distance between the downwind position, *x*, and the most rearward edge of the obstacle. Although no additional information is contained in the expanded number of inputs, it was found that this approach facilitated learning and resulted in NNs with better accuracy and generality.

The Wakenet model consists of two separate feedforward backpropogation networks: one that predicts R_V and one that predicts R_I. This approach was found to result in improved accuracy compared to a single NN that predicted both outputs. Each NN contained an input layer, two hidden layers, and an output layer. The first and second hidden layers had 40 and 20 hidden neurons, respectively. The tan-sigmoid transfer function was used in both hidden layers, while a purely linear transfer function was used in the output layer. Based on trial and error testing, the fastest and most accurate training algorithm for this application was found to be the Levenberg-Marquardt training function, which is often the fastest backpropogation algorithm in the MATLAB NN Toolbox (Demuth 2000).

The performance function is used to evaluate network performance. It is based on the following quantities, which are used to evaluate accuracy and generality

$$e_i = t_i - y_i \tag{1}$$

$$MSE = \frac{1}{N}\sum_{i=1}^{N}(e_i)^2 \tag{2}$$

$$MAE = \frac{1}{N}\sum_{i=1}^{N}|e_i| \tag{3}$$

The error e_i at point i is defined in Eq. (1) as the difference between the target t_i (here, R_V or R_I as measured in the wind tunnel) and the NN prediction at that point, y_i. The mean squared error (MSE) defined in Eq. (2) is the average of the error squared. N is the total number of training data points. The mean absolute error (MAE) defined in Eq. (3) is the mean of the absolute value of the error. MSE was chosen over MAE to evaluate error during training because MSE weights large errors more heavily. Another important term in the performance function is the mean square weight (MSW), the mean of the network weights squared.

$$MSW = \frac{1}{n}\sum_{j=1}^{n}(w_j)^2 \tag{4}$$

The total number of weights in the network is n, and w_j is the value of weight j. Weights quantify the strength of the connection between each pair of neurons. The majority of parameters which

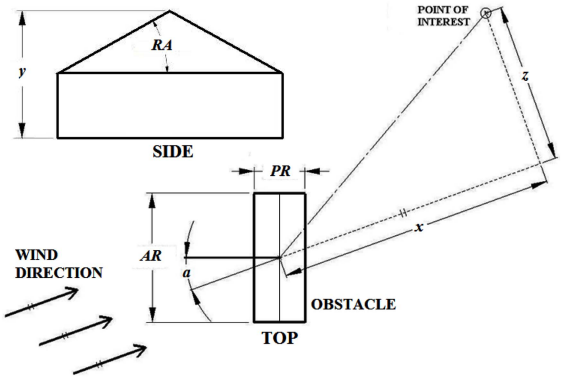

Fig. 1 Definitions of the seven model inputs

make up the neural network are weights. Smaller weights and biases force the network response to be smoother and less likely to overfit (Demuth 2000). A lower MSW typically means that network generalization is better, as was found to be the case here. The Bayesian regularization performance function F was used when training these networks, which means that F is a combination of MSE and MSW. By considering both terms, the network will tend to become more accurate (by reducing the MSE) as well as more general (by reducing the MSW). Another advantage of the Bayesian regularization performance function is that it provides a measure of how many network parameters (weights and biases) are being effectively used by the network (Demuth 2000). This was used to check that the network is an appropriate size. Both final Wakenet networks had 1401 parameters, 1390 of which were being effectively used.

Because network weights and biases are initialized randomly, it was necessary to train and compare many networks in order to obtain the best possible results. The final R_V and R_I NNs were trained for 200 and 95 epochs, respectively.

2.2 Experimental

2.2.1 Wind tunnel testing

Wind tunnel experiments were conducted to collect training and validation data for the neural network-based model. All tests were performed in the University of Guelph Engineering Boundary Layer Wind Tunnel (BLWT), a 9.7 m long open circuit wind tunnel with a square 1.2 m × 1.2 m cross section (Fig. 2). All velocity measurements were taken using one dimensional TSI-1210 hot film anemometers, sampling at 1000 Hz. The sensing length of each hot film probe is 0.51 mm (TSI Incorporated 2008) which is a minimum of one percent of obstacle height. Each hot film probe was calibrated prior to testing using an automatic TSI calibrator. All testing took place within four months of the probes being calibrated. Probes were not recalibrated during or after the wind tunnel experiments, however during testing probe resistance was verified in still conditions at the beginning of each test.

Measurements were made using two hot film anemometers. The first was located in the test section on a ceiling-mounted three-dimensional traversing system that allowed positioning at any location around and downwind of model obstacles. A second hot film was located at a fixed point 3 m upwind of the test section (Fig. 2). Mean velocity and turbulence intensity measurements made in

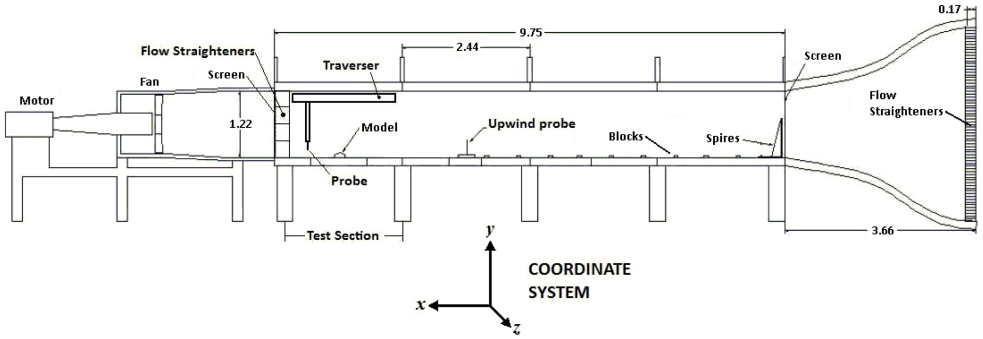

Fig. 2 University of Guelph boundary layer wind tunnel. Dimensions are in m

the test section were normalized by the concurrent upwind measurements to reduce uncertainty associated with long time period unsteadiness in the tunnel. Probe position was tracked in the x and z directions based on grid points on the wind tunnel floor. A sighting ruler integrated in the traversing system was used to measure probe height y.

Model obstacles in the wind tunnel were wooden with sharp edges and rough surfaces. Model dimensions were accurate to 0.5 mm. Table 1 summarizes the unique obstacles used for wind tunnel tests in this study. Obstacle name refers to the shorthand used to describe the obstacle. Category refers to the main use of measurements made in the obstacle`s region of influence. There are three categories of obstacles. Data from `training` obstacles was only used to train the neural networks, while data from `comparison` obstacles was also used to validate wind tunnel measurements against field experiments or results in the literature. Data from the three `validation` obstacles was used exclusively to evaluate the model's generality and was not used for NN training.

A small hole was drilled at the centroid of the bottom of each obstacle, to a depth of roughly 35 mm, such that the hole was not exposed to the wind. Obstacles were secured in place using a steel dowel, and were rotated about this dowel pin to vary orientation angle a while ensuring the center of the obstacle stayed fixed at the coordinate system origin.

A thick turbulent boundary layer was created using techniques commonly employed in BLWT studies (for example, see Lemberg, 1973, Counihan *et al*. 1974, Snyder 1981, Musselman 1996). A mesh screen located at the wind tunnel inlet covers the entire cross section. After testing a range of roughness configurations, the BLWT was outfitted with three 0.8 m tall triangular spires immediately downwind of the inlet. Rows of four evenly distributed small wooden blocks (14 cm long by 8 cm wide by 2 cm high), spaced at 30 cm (1 ft) intervals extended from the tunnel inlet to roughly 4 m in front of the model location. Downwind from this point, the BLWT floor was covered with rough plastic paneling originally intended for diffusing light in fluorescent fixtures, with a characteristic roughness element height of 2 mm.

It was found experimentally that the transition from roughness blocks to panels 4 m upwind of the model reduced longitudinal variation in wind velocity at the test section, resulting in a more consistent boundary layer profile in the test section. Placing the transition closer than 4 m resulted in a less consistent profile at model heights, likely due to the wakes from individual roughness blocks reaching the model. The plastic paneling was intended to be of comparable roughness to the blocks, consisting of more but smaller roughness elements, so while an internal boundary layer is expected to begin at the transition point, it should be of relatively small magnitude. It is thought that this change in surface roughness is a minor source of experimental error. To minimize the

Table 1 Summary of obstacles used in the wind tunnel

Obstacle name	Purpose	AR	PR	RA	*h* (mm)	Number of measured points	Number of profiles
0.5-1 block	Training	0.5	1	0°	50	328	41
Cube	Training, Comparison	1	1	0°	100	632	79
2-1 block	Training	2	1	0°	50	584	73
2-1-15 block	Training	2	1	15°	50	330	41
2-1-30 block	Training	2	1	30°	50	330	41
2-1-45 block	Training	2	1	45°	50	330	41
3-1 block	Validation	3	1	0°	50	106	12
3-2-15 block	Validation	3	2	15°	50	56	7
4-1 block	Training	4	1	0°	53	669	83
4-2 block	Training	4	2.74	0°	50	306	38
5-1-36 block	Validation	4.81	0.85	36°	52	149	15
6-1 block	Training	6	1	0°	50	70	7
9-1 block	Training	9	1	0°	50	268	28
Two-dimensional wall	Training, Comparison	24	0.04	0°	50	56	7
Large wall	Training, Comparison	2.07	0.16 at base 0.04 at top	0°	100	60	NA
Small wall	Training, Comparison	1.03	0.16 at base 0.04 at top	0°	100	60	NA
Trailer block	Comparison	4.73	0.83	0°	50	95	NA
Hansen block	Training, Comparison	2.44	0.75	0	50	44	4

impact of any possible longitudinal variation in the flow, measurements were taken at the same locations with and without the obstacles in place, and any errors in the wake measurements due to this effect should be small (Counihan *et al*. 1974). After the test section, a grid of flow straightening vanes, followed by two screens, span the tunnel, ahead of the diffuser and fan.

Fig. 3 shows measurements made in the undisturbed boundary layer in the wind tunnel compared to reference values. Undisturbed field measurements are also shown, scaled to the wind tunnel.

The undisturbed mean velocity profile in the wind tunnel agrees fairly well with the ASCE 7 reference velocity curve (Zhou 2002). The wind tunnel velocity profile shows less shear than that measured in the field, with power law exponents of 0.17 and 0.23, respectively. Many different combinations of roughness elements were investigated in the tunnel. The configuration selected showed the greatest similarity to the ABL. The inability to exactly replicate the ABL is an inherent source of experimental error in wind tunnel studies (Snyder 1981).

The undisturbed turbulence intensity profile does not match well with the ASCE 7 reference profile; however, the two curves show similar trends, and both curves show large turbulence

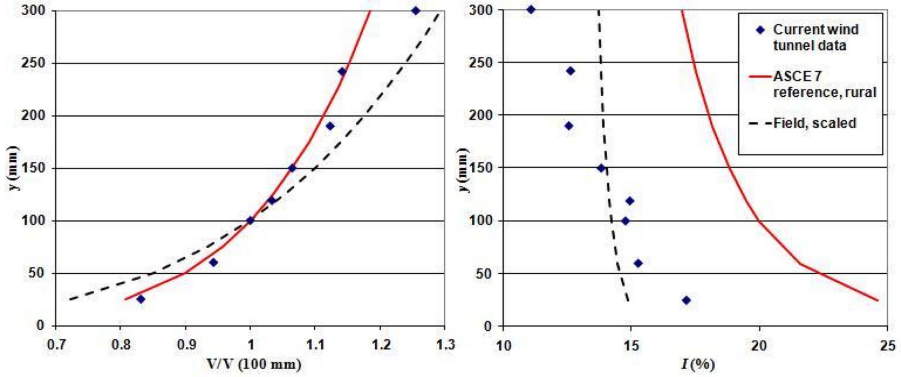

Fig. 3 Comparison of wind tunnel unsheltered profiles to reference profiles for a rural area. (a) Shows mean velocity profiles, including a power law fit derived from measurements taken at the field site and (b) shows mean turbulence intensity profiles

intensity values. Turbulence intensity could be increased by adding a fourth spire, but when this was done, the boundary layer became non-uniform in the lateral direction at the test section, whereas with three spires the flow was very nearly fully developed and laterally uniform in the test section. With the configuration used, the spanwise variation of longitudinal velocity was 1.8% on average, with greater heights seeing less spanwise variation.

Some data scatter is evident in the wind tunnel profiles shown in Fig. 3. This scatter is caused by a combination of uncertainty in the measurements and unsteadiness in the wind tunnel, and is characteristic of this wind tunnel. Based on an examination of a large number of measured profiles, the tunnel boundary layer was found to roughly follow a power law profile.

The 'scaled' field profile was obtained from an 18 m meteorological mast which was located in the same open field as the obstacle tests. This mast was set up and maintained by the authors as part of another experiment. The field data profiles were measured for the open sectors without an obstacle in place. Measurement heights of 5 m, 10 m, and 18 m were used to determine the mean velocity and turbulence intensity power law profiles shown in Fig. 2.

A reasonable ratio of obstacle height h to boundary layer thickness δ must be maintained in the BLWT. In the range of h/δ explored by Lemberg (1973), from $0.17 - 0.25$, this ratio did not have an effect on the rate of decay of maximum velocity deficit in the wake. Counihan *et al*. (1974) and Hansen *et al*. (1975) also concluded that when h/a is small, it is not a significant factor. The wind tunnel simulation criteria specified by Counihan *et al*. (1974) were followed here, which state that $k << h << \delta$, where k is the height of roughness elements. Values of, k, h, and δ were approximately 2 mm, 50 mm, and 400 mm respectively in the test section.

The sampling period for all measurements was 32.768 seconds (arrived at by specifying that 32×2^{10} points should be measured at a frequency of 1000 Hz). This sampling time was determined by taking three 40 minute samples in the wind tunnel. Moving averages were calculated using a range of sampling times (from 8 seconds to 256 seconds). 32.8 seconds was found to be an optimal balance between the reduced number of samples that could be collected in the wind tunnel if a longer sampling time were used, and the increased variability (scatter) in the data that was present when shorter sampling times were used due to unsteadiness in the flow. Here, unsteadiness refers to the variation of mean wind speed on time scales larger than the 32 second averaging time. The

spectral content of the flow was investigated to examine this variation in mean wind speed. It was found that the main energy containing scales were between 1 Hz and 3 Hz, with no evidence of domination by a low frequency component. This is consistent with the observation that the variation of (32 second) mean wind speed was only about 1.0%, on average. Hence, the unsteadiness component is small, but not negligible.

Free stream wind speed was generally 9.3 m /s. Measurements were only made away from the wind tunnel side walls, in the centre half of the tunnel. Obstacles were also only located in the centre half of the tunnel. (The one exception to this was the two-dimensional wall, which spanned the tunnel.) Overall tunnel blockage was maintained at less than 5% including the traversing system. Typically, tunnel blockage was 1 to 2%, depending on the obstacle. The boundary layer thickness along the walls and roof was estimated at 20 cm, based on the measured boundary layer thickness above the floor when no roughness elements or spires were in place.

A careful testing procedure was followed in the wind tunnel. Using the traversing system, the hot film probe was moved to the point of interest, and the flow at both probe locations was measured. The velocity ratio R_{V1} is the ratio of the mean unsheltered wind speed at the point of interest, $\overline{V_1}$, to the mean wind speed at the upwind probe over the same time period, $\overline{V_{0.1}}$

$$R_{V1} = \frac{\overline{V_1}}{\overline{V}_{0.1}} \tag{5}$$

$$R_{I1} = \frac{I_1}{I_{0.1}} \tag{6}$$

Similarly, Eq. (6) defines the turbulence intensity ratio R_{I1} as the ratio of the unsheltered turbulence intensity at the point of interest, I_1, to the turbulence intensity at the upwind probe over the same time period, $I_{0,1}$. The zero in the subscript '0,1' indicates that the measurement was made at the upwind probe, while the one indicates that the measurement was made without the obstacle in place.

The obstacle was then put in place, and the flow was again measured. The normalized sheltered mean wind speed R_{V2} and turbulence intensity R_{I2} are then

$$R_{V2} = \frac{\overline{V_2}}{\overline{V}_{0.2}} \tag{7}$$

$$R_{I2} = \frac{I_2}{I_{0.2}} \tag{8}$$

The subscript '2' indicates that the measurements were taken while the obstacle was in place. Using these values, the desired Wakenet model output ratios for a specific point, R_V and R_I, are

$$R_V = \frac{R_{V2}}{R_{V1}} \tag{9}$$

$$R_I = \frac{R_{I2}}{R_{I1}} \tag{10}$$

R_V is essentially the velocity normalized twice, since it is first normalized by measurements made at the reference point over each sample time, and then the sheltered value is normalized by the corresponding unsheltered value. R_I can be thought of as the thrice normalized root mean square velocity, since turbulence intensity is itself a normalized quantity. Using 95% confidence intervals, the uncertainties of R_V and R_I are estimated to be 2.9% and 9.3%, respectively, following the uncertainty propagation methods of Coleman and Steele (1989). A large part of these uncertainties is related to the unsteadiness of the wind speed in the tunnel.

In practice, each sheltered measurement was not directly preceded by an unsheltered measurement. Rather, a full unsheltered vertical profile was measured first, followed by a full sheltered profile. Often, an unsheltered vertical profile would be measured at the (x, z) location of interest, followed by multiple sheltered profiles at the same location, each with a unique obstacle or obstacle orientation. To maintain consistency, sheltered and unsheltered profiles were taken without changing the free steam wind tunnel speed. To avoid potential anemometer drift, the length of time between measuring a sheltered and unsheltered profile did not exceed two hours, and was typically much less.

In total, 4473 unique R_V and R_I values were obtained for the 18 obstacles investigated. Each of these measured "points" consists of a value for each of the seven inputs, and the corresponding R_V and R_I values. A total of 517 vertical profiles were measured, with each vertical profile typically consisting of 8 points, although this varied depending on the obstacle. For example, because the wake of the 9-1 block extended to a greater height than the wakes of most other obstacles, several of the vertical profiles in its wake consisted of 10 points instead of 8. A small number of horizontal profiles were also taken.

2.2.2 Field experiment

A field experiment was conducted to obtain wind speed and turbulence measurements in the wakes of full scale obstacles exposed to an actual rural ABL to provide data for validating wind tunnel simulations and model predictions. The experiment was located in a large, flat open field in a rural area southwest of Kitchener, Ontario, Canada (43°18' N, 80°33' W). Prevailing winds are from west-southwest. Six towers were equipped with anemometers and erected around an obstacle (see Fig. 4). This arrangement allowed measurement of the obstacle wake for a wider range of wind directions and model orientations. The upwind fetch was great enough (more than 50 obstacle heights) in all wind directions of interest (180° to 360°) that interference effects from other obstacles far upwind would be minimal, or at the very least, typical of a site where a small turbine might be installed.

As seen in Fig. 4, ten anemometers were used in total: three Campbell Scientific CSAT3 three-dimensional sonic anemometers, one RM Young 81000 three-dimensional sonic anemometer, and six NRG #40 C cup anemometers. A Campbell Scientific CR-1000 datalogger was used for data collection. The sonic anemometers were sampled at 20 Hz, while the cup anemometers were sampled at 2 Hz. Over the course of the experiment, three structures were used as obstacles, as described in Table 2.

One month of data was collected without an obstacle in place to quantify any baseline variation in velocity or turbulence intensity between the anemometers, as a function of wind direction. Recorded data was quality controlled and averaged over 30 second periods. A short averaging period was used to ensure strong, consistent wind throughout the sample. While a 10 minute average would have been preferable in terms of including the lower frequency components of turbulence intensity,

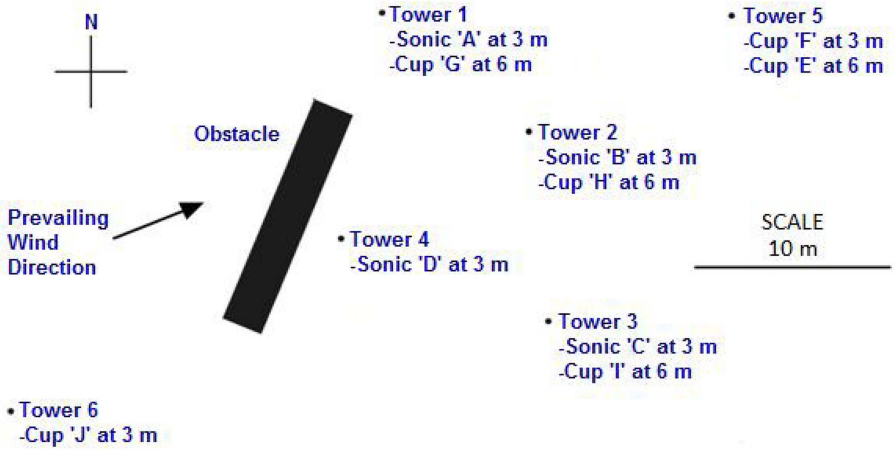

Fig. 4 Layout of field experiment, with the trailer as the obstacle

Table 2 Summary of obstacles used in the field experiment

Obstacle	Large wall	Small wall	Box trailer w/ filled bottom
Height	2.48 m	2.48 m	2.6 m
Width	5.14 m	2.57 m	12. 3 m
Depth	0.4 m at base	0.4 m at base	2.16 m
	0.1 m at top	0.1 m at top	
Days of useful data	18 days	31 days	22 days

it was found that compared to 30 second periods, there were far fewer 10 minute periods with strong consistent winds over the four month measuring period. Strong, directionally consistent winds were needed to measure the effect of the obstacle accurately. The use of the 30 second period resulted in a larger number of samples, which reduced the uncertainty in the results.

Data was filtered to eliminate points with a low mean wind speed (less than 4 m/s), or high standard deviation of wind direction (greater than 12°). This ensured that all wake measurements were based on strong, consistent winds. The specific filtering cut-off values used were determined by trial and error; the optimal values were those where more stringent cut-offs resulted in little change in mean velocity and turbulence ratios values. Recall that the calculation of R_V and R_I requires a sheltered and an unsheltered measurement. It was assumed that without the influence of the obstacle, the mean flow at each tower location would be the same as the upwind flow, taking into account the baseline ratios. For a given wind direction and sensor of interest, any sensor at the same height that is not sheltered could be used as the reference sensor.

R_V and R_I were calculated for each averaging period. These ratios were then sorted by wind direction into bins. A bin size of 10° was used. Final $\overline{R}_v$ and $\overline{R}_1$ values were calculated for each bin by taking the mean of all the sample values from that bin that met the filtering criteria. To ensure the certainty of field measurements, 95% confidence intervals were estimated for each sensor, using each obstacle, for each wind direction.

3. Results and discussion

3.1 Comparison of wind tunnel and field experiment results

Wind tunnel results were compared to measurements from the field experiment to validate the wind tunnel simulations. It should be noted that the wind tunnel and field experiments did not measure exactly the same quantities. Field experiment results for R_V, R_I and wind direction are based on the downwind and lateral velocity components. Wind tunnel results are inherently based on the downwind and vertical velocity components, due to the configuration of the hot film. Since downwind velocities are generally at least an order of magnitude greater than lateral or vertical components, in both experiments, this discrepancy should not affect the validity of directly comparing results. (An exception to this is at sonic 'D', where the lateral velocity component may be of the same order as the freestream downwind velocity). Geometrically similar models of the full scale obstacles (described in Table 1), at scales of 1:25 and 1:52 for the walls and trailer block respectively, were created and tested in the wind tunnel. Measurements were made in the wind tunnel at locations corresponding to anemometer locations in the field.

Field results were compared to wind tunnel results for each anemometer location and obstacle by looking at the mean absolute difference (MAD) between the two experiments. Comparisons included in this section were specifically selected to illustrate the main findings of the field study. For a more in-depth analysis, see Brunskill (2010). R_V values measured in the wind tunnel generally compared well with those measured in the field, although wind tunnel measurements were often slightly higher, as seen for example in Fig. 5.

In a few cases, there were large discrepancies between wind tunnel and full scale results for R_V. As illustrated in Fig. 6, an example of this occurred at anemometer C for wind from the 10° bin centered at 305° when the trailer was present. The mean R_V value based on full scale measurements was 0.66, based on 96 suitable averaging periods, with a 95% confidence interval of less than 0.05. The corresponding R_V in the wind tunnel was 0.88, which was verified by repeating the measurement on three different occasions. This discrepancy may have been caused by a small difference between the actual geometry of the trailer and the wind tunnel model of the trailer. The end of the trailer was enclosed with a flexible fabric door, while the model of the trailer was a solid wooden block. Alternatively, there may have been an important genuine difference between the flows observed in the wind tunnel and the field in this particular case. In BLWT studies, it is often assumed that the flow around sharp-edged objects is independent of Reynolds number *Re*, above a critical value range of 2 to 3×10^3 (Snyder 1981). However, *Re* dependence in the far wake may depend on the nature of the vortices originating from the obstacle. Hansen *et al*. (1975) suggest that the *Re* dependence of vortex decay rate may be greater than the *Re* dependence of a flow field which is largely irrotational.

In the case described above, the obstacle orientation a was 12°, and standing vortices were likely

Table 3 MAD values for R_V and R_I for the large wall, small wall and trailer

Obstacle	R_V (% MAD)	R_I (% MAD)
Large wall	4.9%	11.6%
Small wall	2.9%	7.4%
Trailer	5.3%	13.1%

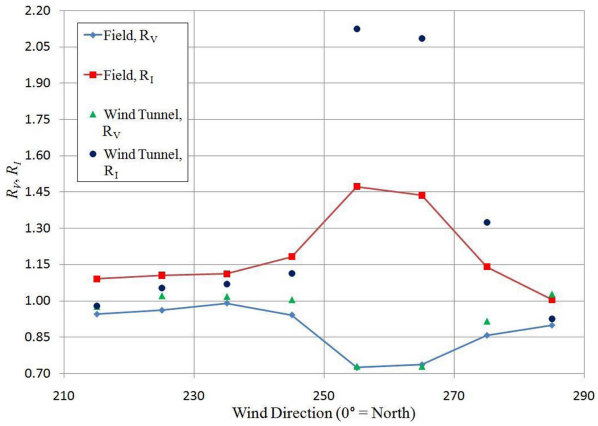

Fig. 5 Variation of R_V and R_I at anemometer F, in the wake of the trailer

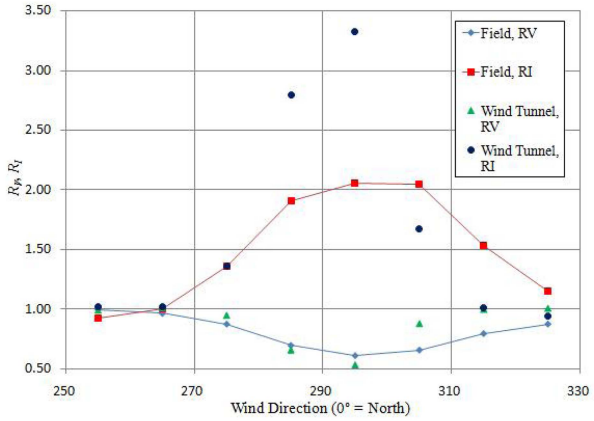

Fig. 6 Variation of R_V and R_I at anemometer C, on tower 3 at a height of 3.02 m, in the wake of the trailer

formed from the prominent corner of the obstacle in both the wind tunnel simulation and the full scale experiment. Flow in the vicinity of these vortices may have a greater dependence on *Re* than flow elsewhere in the wake. Fig. 5 shows that at anemometer F, when wind is coming from 255° and 265°, full scale results agree well with wind tunnel results for R_I. Since standing vortices are expected to be present for both these wind directions, this is evidence that *Re* dependence is still valid in this case, which supports the explanation regarding the flexible fabric door. On the other hand, this apparent discrepancy is also evident at the same wind direction and measurement point for the large wall, as seen in Fig. 7. Clearly there is conflicting evidence; further investigation is required to conclusively demonstrate the validity of assuming that R_V is independent of *Re* in the far wake in all cases.

Based on a height of 50 mm (the most common obstacle height) and the mean incoming wind speed at 50 mm, the *Re* of the flow around an obstacle in the wind tunnel was 2.5×10^4. Lim *et al.* (2007) studied the *Re* dependence of the flow around a cube in a BLWT, spanning a *Re* range of 1.86×10^4 to 4.09×10^5. Lim *et al.* (2007) found that for classes of bluff body flow with no concentrated vortex fields, local mean velocity fields were not *Re* dependent. However, fluctuating

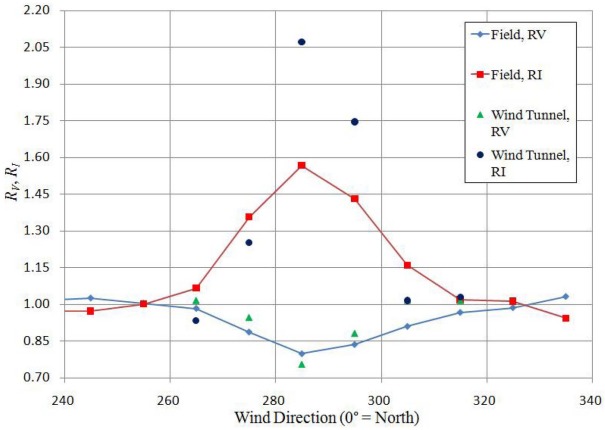

Fig. 7 Variation of R_V and R_I at anemometer C, on tower 3 at a height of 3.02 m, in the wake of the large wall

quantities did show a dependence on *Re*. This agrees with findings of the current study; comparing wind tunnel to full scale results, normalized mean wind speeds agree well, while turbulence intensities do not. Lim *et al*. (2007) also found that when strong vortices existed, mean quantities were also dependent on *Re*. This was not consistent with current results; aside from the possible exception noted above, the presence of vortices did not appear to have an effect on the *Re* dependence of normalized mean wind speeds. However, this may be explained by considering that Lim *et al*. were investigating the flow in the immediate vicinity of a cube, while the current investigation focused mainly on the far wake region.

As seen in Figs. 6 and 7, R_I values were greater in the wind tunnel than in the field. This can likely be attributed to how the turbulence intensity is defined differently in the field and in the wind tunnel. The 30 second averaging period used in the field results in the absence of lower frequency turbulence components. However, it is felt that a comparison of the two differently defined turbulence intensities is still of interest, and that the predictions of R_I as defined in the field experiment would still be helpful when micrositing a small wind turbine.

The greatest discrepancy in R_V was seen at sonic anemometer 'D', which was closest to the obstacle. This is thought to be because of the sensor's close proximity to the obstacle; it is in the near wake region, where lateral velocity components may be on the same order as the freestream downwind velocity components. Results from this sensor are of interest, although the main area of interest in this project is the far wake region.

In general, a model developed from BLWT data can potentially make R_V predictions of acceptable accuracy, but R_I will tend to be overestimated by a model based on wind tunnel data, in some cases by a large margin. This effectively makes the model conservative when making predictions regarding the turbulence wake of an obstacle.

3.2 Predicting wind speed distribution

The probability density function (PDF) of wind speed at the site must be considered to make accurate predictions of a turbine's energy output over a given period of time. At a sheltered location, the wind speed velocity distribution will be different from that at an unsheltered point. Fig. 8 shows how the PDF at cup anemometer 'C' compares to the PDF at cup anemometer 'A',

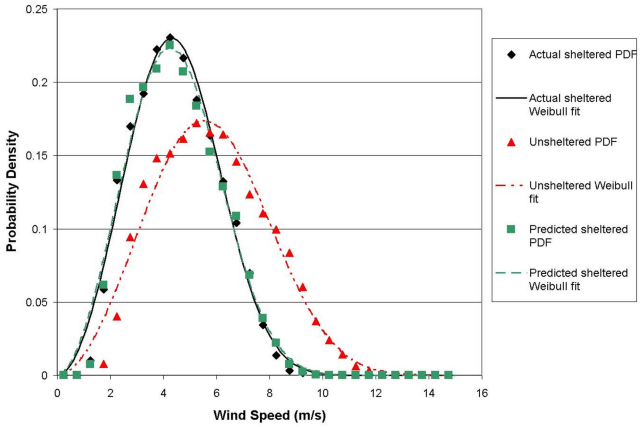

Fig. 8 PDFs and Weibull fits of unsheltered data, sheltered data, and predicted data

when the wind is coming from sector 24 (between 230° and 240°, chosen because it had the most available data, 4713 samples). In this case, anemometer A is sheltered by the trailer block, while anemometer C is unsheltered. Data samples used to create this figure were not filtered for wind speed or standard deviation of wind direction. Also shown in Fig. 8 are best fit Weibull distributions for both locations.

An R_V value of 0.78 was determined for anemometer A with this wind direction. Recall that R_V is essentially a correction factor. To try to predict the effect of sheltering on the PDF of wind speed, all wind speeds measured at the unsheltered sensor were multiplied by this correction factor, creating a new set of 'sheltered' wind speeds. The PDF was calculated from this new data set; this is also shown in Fig. 8. The predicted sheltered PDF is very close to the measured sheltered PDF. This result is significant because it supports that the wind speed probability distribution at a sheltered point can be predicted based on (i) the unsheltered PDF, which is given in most wind maps, and (ii) a single correction value for that point, R_V. This is also evidence that the correction factor R_V is independent of *Re*, since the single correction factor appears to be valid at all wind speeds (and *Re*).

3.3 Comparison of model predictions to wind tunnel results

The error statistics for predictions of R_V and R_I from the final Wakenet NNs are shown in Table 4 for each of the four data sets discussed previously. As would be expected, the training data set

Table 4 MSE and MAE of the final R_V and R_I NNs

	R_V		R_I	
Data set	MSE	MAE	MSE	MAE
Training	$1.56 \cdot 10^{-4}$	0.8%	$2.85 \cdot 10^{-3}$	2.6%
Validation	$2.99 \cdot 10^{-4}$	0.9%	$4.54 \cdot 10^{-3}$	2.9%
Pure validation	$1.42 \cdot 10^{-3}$	3.1%	$4.82 \cdot 10^{-2}$	11.0%
Pure validation, far wake	$2.98 \cdot 10^{-4}$	1.3%	$5.72 \cdot 10^{-3}$	5.3%

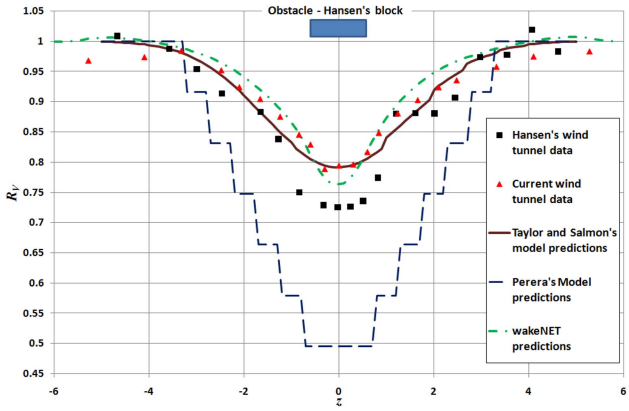

Fig. 9 Lateral R_V profiles in the wake of Hansen's block at x = 7.55, y = 0.94, a = 0°

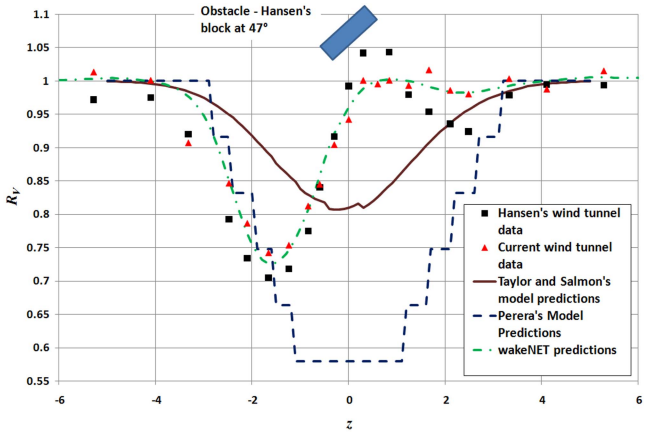

Fig. 10 Lateral R_V profiles in the wake of Hansen's block at x = 7.55, y = 0.94, a = 47°

shows the lowest MSE. The pure validation data set showed the greatest error by far, but it appears to perform much better in the far wake than the near wake. The MSE of the far wake subset is very close to the MSE of the validation data from the training pool, and both MSE values are of the same order of magnitude as the MSE of the training data, indicating that the neural networks show strong generality in the far wake region.

Fig. 9 shows results for the lateral R_V profile in the wake of Hansen's block (described in Table 1) at x = 7.55, y = 0.94. The wind tunnel results of Hansen *et al.* (1975) predict slightly greater velocity deficits than those measured as part of this study, especially in the center of the wake, but overall the agreement is reasonably good. Wakenet predictions are very similar to current wind tunnel data and predictions made by Taylor and Salmon's model, while Perera's model greatly underestimates R_V.

The block used by Hansen *et al.* was rotated to a = 47° and the lateral R_V profile was measured at x = 7.17, y = 0.94, as shown in Fig. 10. Both sets of wind tunnel data predict that the maximum velocity deficit occurs nearly 2h from the obstacle centerline. Wakenet is able to predict this feature accurately, in terms of both the location and magnitude of the peak. Taylor and Salmon's model is unable to predict either the location or the magnitude of the maximum velocity deficit because the assumed Gaussian lateral similarity profile is no longer valid; the wake is clearly not symmetrical

about $z = 0$. Current wind tunnel measurements at other orientation angles confirm that the form of the lateral R_V profile is highly dependent on the orientation of the obstacle. It can be stated that generally the forms of lateral R_V and R_I profiles are dependent on the obstacle's geometry, as presented to the prevailing wind. Since the model developed here is entirely empirical, it is able to accurately predict these asymmetrical profiles because they are inherently part of the training data. It was also observed that the mean wind speed on the center line is nearly fully recovered, and in fact, Hansen *et al*. (1975) observed a velocity excess of nearly 5%. Both Perera's model and Taylor and Salmon's model predict that the mean wind speed will be at a minimum on the centerline.

3.4 Validation

Fig. 11 shows how NN predictions of R_V compare to wind tunnel data at one (x, z) location in wakes of the pure validation test obstacles. Recall that these obstacles were not used to generate training data; these predictions are all based on the relationship learned from measurements of the wakes of other obstacles. The validation obstacles were designed such that one or more of their geometric characteristics was not present in any of the training data. In general, the R_V predictions in Fig. 11 are not as accurate as those in Figs. 9 and 10. Although the predicted profile for the 5-1-36 block overestimates the velocity deficit in the wake, overall, velocity predictions for this obstacle are acceptable, especially above $y = 1$. The measured 3-1 block profile has also been predicted well. R_V predictions for the 3-2-15 block are not accurate at lower heights; the velocity deficit is overestimated, especially at $y = 0.9$. Higher above ground, prediction accuracy improves. Wind tunnel measurements indicate that at this (x, z) location, for this a value, the 3-1 block creates a greater velocity deficit than the 3-2-15 block, which is the opposite of the effect of PR at other locations. It is possible that this is caused by the different RA values, but typically RA does not have a large effect at this distance from the obstacle. This finding illustrates the complexity of the problem; different obstacle characteristics will have different effects at different points in the wake. For all three obstacles, predictions are better at heights where $y > 1$. This is important, since the

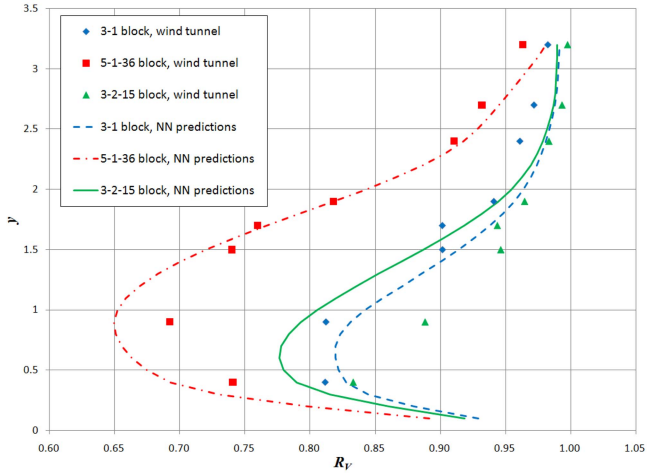

Fig. 11 Variation of R_V with height at $x = 12$, $z = 3$, $a = -40^{o}$ in the wakes of three obstacles used purely for validation

main region of interest when siting small wind turbines is at heights greater than that of the obstacle.

3.5 Comparison of model predictions to full scale results

Wakenet predictions were directly compared to full scale measurements for the trailer block. Since neither the wind tunnel data for the trailer block simulation nor the field data was used to train the NN, this should provide a good indication of how Wakenet will perform for new full scale obstacles. The MAD between Wakenet predictions of R_V and values measured in the field is 6.9%. This can be thought of as the model's prediction error. The greatest discrepancy between predictions and field data tends to occur at data points that were measured at anemometer D, which was closest to the obstacle, as seen in Fig. 4. When this anemometer is not considered, MAD is reduced to 5.3%. This is thought to be a more accurate estimate of MAD for values in the far field. Another way of estimating the mean error associated with the model is to combine the mean difference between full scale measurements and the wind tunnel simulation (4.3%) with the error associated with model predictions of wind tunnel results (1.3%). This results in an overall mean error estimate of 4.5%. The mean of the two estimates of error when predicting R_V is 4.9%.

The MAD between Wakenet predictions and field measurements of R_I is 20.0%, which is quite high. When data from anemometer D is not considered, the mean absolute difference decreases to 13.6%. Most of this apparent discrepancy stems from the difference in how R_I is defined in the wind tunnel and in the field, as discussed previously. As with R_V, mean error in the model can also be estimated by combining the uncertainties associated with going from the model to the wind tunnel for new obstacles, 5.3%, and the wind tunnel to the field, 10.7%, to obtain a total mean uncertainty of 11.9%. The mean error of Wakenet predictions of R_I is estimated to be 12.8%.

It should be kept in mind that the above estimates of accuracy do not fully describe the performance of Wakenet. In fact, it is difficult to characterize the model's performance using a single value, since the validity of the wind tunnel simulation (from which all training data was generated) depends greatly on the location of the point of interest relative to the obstacle. This is evident in Fig. 5, where for R_I, the difference between wind tunnel and field results is clearly much greater in the center of the plot (between 250° and 270°) than outside of this range.

Wakenet prediction accuracy will also depend on the degree of similarity between the obstacle and the obstacles used for training. Further model training and validation using additional measurements would improve the model, and also allow for a more thorough evaluation of its accuracy and generality.

4. Conclusions

The flow field was investigated for a range of typical building-like obstacles in a BLWT, with emphasis on the obstacle wake region. Comparisons to field measurements suggest that the mean velocity wake of a full scale obstacle can be accurately simulated in a BLWT. The correct magnitude of the obstacle turbulence intensity wake is more difficult to simulate. Turbulence intensity measurements made in the wind tunnel were generally greater than those made in the field. Wind tunnel simulations were more accurate for flow properties in the far wake than in the near wake. In general, *Re* independence appears to be valid for the velocity wake, but not for the

turbulence intensity wake, at least over the *Re* range used in this study. There is some evidence that locations in the wake strongly influenced by standing vortices may be more dependent on *Re* than locations where effects from standing vortices are insignificant.

The *AR* of an obstacle has a major effect on the extent and magnitude of the obstacle's wake. An obstacle with a larger *AR* will produce a much larger downwind region of decreased mean wind speed and increased turbulence intensity than an obstacle with a smaller *AR*. The orientation of the obstacle relative to the wind direction has a large effect on standing vortex formation, and strongly affects mean velocity and turbulence levels throughout the wake. Wakes are only symmetrical for special cases of model orientation; specifically, when the obstacle geometry is symmetrical about the wind direction. Increased *PR* was found to often be associated with an increase in the magnitudes of wake effects, although there were exceptions. The effects of *PR* and *RA* on wake properties strongly depend on obstacle orientation and the position of interest in the wake.

A new NN-based model called Wakenet has been developed that can predict the mean wind speed and turbulence intensity in the wake of a simple solid obstacle exposed to a rural ABL. Through a comparison with new field data, it is estimated that predictions of R_V and R_I will have a mean error of 5.0% and 12.8%, respectively, at points that are in the far wake and at heights greater than that of the obstacle. To improve model performance, predictions of mean wind speed and turbulence intensity are made using two separate neural networks. The main source of uncertainty in neural network predictions is believed to be variations in the wind tunnel simulation; while generally valid, it is inherently different from an actual ABL. Model predictions will be most accurate for obstacles similar to those used to train the model; however, predictions made using new obstacles still tend to show fairly good accuracy, especially in the far wake region.

The new model has only been validated for an ABL typical of open, rural areas, and should not be used in an urban setting. Similarly the current model is limited to areas with flat terrain.

The ease of retraining the model as new or refined wind tunnel data becomes available is considered to be an asset of the neural network approach, as is the ease of use of the completed model. In the future, it may be possible to improve model predictions in the near wake and above obstacle regions through the creation of a separate NN for each region, utilizing additional inputs as appropriate. Future studies could evaluate the benefits of using a NN approach, such as that described here, compared to a simple CFD approach when modeling the flow around obstacles.

Acknowledgements

Mr. Brunskill was supported as a graduate researcher by the Ontario Centres of Excellence, Centre for Energy. The Canada Foundation for Innovation, and the Ontario Ministry of Research and Innovation, provided funds for the infrastructure used in this study. The authors would also like to thank Ian Nichols and Rob Danford of Weather Innovations, and Al Paulissen and Randy Seager at Wenvor Technologies for their advice and assistance during this study.

References

Bitsuamlak, G.T., Bédard, C. and Stathopoulous, T. (2006), "Effects of upstream two-dimensional hills on design wind loads: A computational approach", *Wind Struct*., **9** (1), 37-58.

Bitsuamlak, G.T., Bédard, C. and Stathopoulous, T. (2007), "Modeling the effect of topography on wind flow using a combined numerical-neural network approach", *J. Comput Civil Eng*., **21**(6), 384-392.
Brunskill, A. (2010), *A neural network-based wake model for small wind turbine micrositing near obstacles*, Masters Thesis.
Chen, Y., Kopp, G.A. and Surry, D. (2003), "Prediction of pressure coefficients on roofs of low buildings using artificial neural networks", *J. Wind Eng. Ind. Aerod*., **91**(3), 423-441.
Coleman, H.W. and Steele, W.G. (1989), *Experimentation and uncertainty analysis for engineers*, John Wiley & Sons, Inc.
Counihan, J., Hunt, J.C.R. and Jackson, P.S. (1974), Wakes behind two-dimensional obstacles in turbulent boundary layers, *J. Fluid Mech*., **64**(3), 529-563.
Demuth, H. and Beale, M. (2000), *Neural network toolbox user's guide*, Version 4. Natick, MA : The MathWorks.
Hansen, A., C., Peterka, J.A., and Cermak, J.E. (1975), *Wind-tunnel measurements in the wake of a simple structure in a simulated atmospheric flow*, NASA STI. Recon Technical Report CR2540.
Khanduri, A.C., Stathopoulos, T. and Bedard, C. (1997), "Modelling wind-induced interference effects using backpropagation neural networks", *J. Wind Eng. Ind. Aerod*, **72**, 71-79.
Lemberg, R. (1973), *On the wakes behind bluff bodies in a turbulent boundary-layer. Boundary Layer Wind Tunnel Laboratory*, University of Western Ontario. London, Ontario, Canada. Ph.D. Dissertation.
Lim, H.C., Castro, I.P. and Hoxey, R.P. (2007), "Bluff bodies in deep turbulent boundary layers: Reynolds-number issues", *J. Fluid Mech*., **571**, 97-118.
Martinuzzi, R. and Tropea, C. (1993), "The flow around surface-mounted, prismatic obstacles placed in a fully developed channel flow", *J. Fluid. Eng-T ASME*, **115**, 85-92.
Musselman, D.D. (1996), *Turbulent wake interactions of multiples structures in an atmospheric boundary layer. boundary layer wind tunnel laboratory*, University of Western Ontario. London, Ontario, Canada : s.n. Ph.D. Thesis.
Perera, M.D. (1981), "Shelter behind two-dimensional solid and porous fences", *J. Wind Eng. Ind. Aerod*., **8**(1-2), 93-104.
Peterka, J.A., Meroney, R.N. and Kothari, K.M. (1985), "Wind flow patterns about buildings", *J. Wind Eng. Ind. Aerod*., **21**(1), 21 -38.
Snyder, William H. (1981), *Guideline for fluid modeling of atmospheric dispersion*, Environmental Sciences Research Laboratory, U.S. Environmental Protection Agency.
Taylor, P.A. and Salmon, J.R. (1993), "A model for the correction of surface wind data for sheltering by upwind obstacles", *J. Appl. Meteor*., **32**(11), 1683-1694.
TSI Incorporated. (2008), TSI Thermal Anemometry Probes Catalog. Available online at http://www.tsi.com/uploadedFiles/Product_Information/Literature/Catalogs/Hotwire_Catalog_2980465.pdf. Accessed Sept. 2009.
Troen, I. and E.L. Petersen. (1989), European Wind Atlas. ISBN 87-550-1482-8. Risø National Laboratory, Roskilde, Denmark.
U.S. Department of Energy. (2005), Small Wind Electric Systems. A U.S. Consumer's Guide. Available online at http://www.windpoweringamerica.gov/pdfs/small_wind/small_wind_guide.pdf. Accessed July 19 2010.
Zhang, A., Zhang, L. (2004), "RBF neural networks for the prediction of building interference effects", *Comput. Struct*., **82**(27), 2333-2339.
Zhou, Y. and Kareem, A. (2002), "Definition of Wind Profiles in ASCE 7", *J. Struct Eng-ASCE*, **128**(8), 1082-1086.

CC